World Journal of Pharmaceutical Science and Research

www.wjpsronline.com

Review Article

ISSN: 2583-6579
SJIF Impact Factor: 6.916
Year - 2026
Volume: 5; Issue: 6
Page: 178-190

EMERGING COMPUTATIONAL APPROACHES IN THE DEVELOPMENT OF BACE1 INHIBITORS FOR ALZHEIMER'S THERAPY: A REVIEW

Dere Aditya Sampat[1], Lokhande Rahul Prakash[2], Gadge Shrutika Pralhad[1], Dongare Tanvi Sopan[1], Gaikwad Sakshi Rajesh[1], Gadekar Sainath Vijaysing[1]

[1]Student, Samarth Institute of Pharmacy, Belhe Maharashtra, India.

[2]Associate Professor, Department of Pharmaceutical Quality Assurance Samarth Institute of Pharmacy, Belhe, Maharashtra, India.

Article Received: 03 April 2026 | | Article Revised: 24 April 2026 | | Article Accepted: 14 May 2026

***Corresponding Author: Dere Aditya Sampat**
Student. Samarth Institute of Pharmacy, Belhe Maharashtra, India.
DOI: https://doi.org/10.5281/zenodo.20443715

How to cite this Article: Dere Aditya Sampat, Lokhande Rahul Prakash, Gadge Shrutika Pralhad, Dongare Tanvi Sopan, Gaikwad Sakshi Rajesh, Gadekar Sainath Vijaysing (2026) EMERGING COMPUTATIONAL APPROACHES IN THE DEVELOPMENT OF BACE1 INHIBITORS FOR ALZHEIMER'S THERAPY: A REVIEW. World Journal of Pharmaceutical Science and Research, 5(6), 178-190.

ABSTRACT

Alzheimer's disease (AD) is a progressive neurodegenerative disorder characterized by cognitive decline and memory loss. A key feature of AD is the accumulation of amyloid beta (Aβ) peptides in the form of extracellular plaques. The amyloid cascade hypothesis suggests that the pathogenesis of AD is initiated by the cleavage of amyloid precursor protein (APP) by β-site amyloid precursor protein cleaving enzyme 1 (BACE1). Numerous therapeutic approaches have been pursued to target BACE1 due to its crucial role in AD. However, the complexity of AD and the localization of BACE1 in the brain have posed challenges, leading to the failure of clinical trials and, in some cases, even exacerbating disease progression. Specifically, the blood–brain barrier (BBB) prevents the entry of many molecules, making BACE1 a difficult target to approach. Recent advancements in BACE1 therapy have shifted the focus from traditional enzyme inhibitor-based therapeutics to modulators, antibody therapy, and gene therapy. These approaches offer several advantages, including the ability to efficiently cross the BBB and provide targeted treatment. In this review, we explore the latest developments in modulators, antibody therapy, and gene therapy targeting BACE1 to combat AD. These approaches offer a promising avenue to mitigate the progression of AD and provide a novel therapeutic strategy.

KEYWORDS: Alzheimer's disease, BACE1 inhibitors, molecular docking, molecular dynamics, virtual screening, QSAR, artificial intelligence, computer-aided drug design, ADMET prediction, blood-brain barrier, drug discovery.

INTRODUCTION

Alzheimer's disease (AD) is a neurodegenerative disease and is the primary cause of dementia, which can be described as a constant, and continuous loss of memory combined with cognitive impairment and change in personality. It is currently one of the chief causes of death and has affected more than 44 million people around the world. AD mainly affects people of old age (>65 years), hence as the demographics of society changes, the prevalence of AD and other age-related dementias increases. Discovery and development of drugs for AD is a tedious process. In 2023 FDA had approved a new category of drug lecanemab, only for people with mild cognitive impairment however studies are stating the patients who received drug are experiencing edema, or fluid formation on the brain Currently there are only six FDA (Food and Drug Administration) approved prescriptions drugs available to treat the symptoms associated with AD. These include Tacrine, Donepezil, Galantamine, and Rivastigmine which are acetylcholinesterase (AChE) inhibitors, Memantine which is an N–methyl-Daspartate receptor antagonist (NMDA), and Suvorexant which is an orexin receptor antagonist.

The brains of AD patients are characterized mainly by two histopathological features, which are amyloid (Aβ) plaques consisting of ß-amyloid (Aß) peptides located outside the cells and neurofibrillary tangles made up of hyper phosphorylated tau protein located within the neurons. Evidence has emerged indicating that Aß peptide and its aggregation forms a vital aspect of the development of AD. BACE1 (ß-secretase) is an aspartic protease mainly present in the central nervous system (CNS) and contained in the presynaptic terminals. It is responsible for generating Aß by breaking down the transmembrane protein APP (ß-amyloid precursor protein. Usually, α-secretase governs proteolytic processing of APP in a healthy brain, however, when α-secretase is inhibited, ß- and γ-secretases take over and bring about the formation of neurotoxic Aß 1–40 and Aß 1–42. Aß 140 and Aß 1–42 aggregate easily and get deposited.

These are the main components of Aβ plaques. The production and deposition of Aß are considered to be the factors leading to pathological changes in AD, such as neurofibrillary tangles, neuron loss, vascular injury, dementia, and many more.

BACE1 is considered a major target for the development of drugs that can decrease cerebral Aß levels for the treatment and prevention of AD. BACE1 inhibition would stop Aß production and curb the occurance of Aß-associated pathologies. Also, the studies on BACE1 knockout mice showed that the initial reports were free of any harsh phenotype and didn't exhibit any pathological abnormalities. Over the last few years, various BACE1 inhibitors underwent clinical assessment. Initially, many BACE1 inhibitors were discontinued during Phase 1 or early Phase 2 trials due to liver, ocular, or cardiac toxicity. Some BACE1 inhibitors such as verubecestat, atabecestat, lanabecestat, and umibecestat advanced well in clinical trials but failed to display improvement in cognition and function in placebo-oriented studies. Elenbecestat was the final BACE1 inhibitor to be discontinued in Phase 3 trials.

BACE1 is a transmembrane protein of the type 1 category. It consists of a sequence of 82 amino acids running C-terminally to the homologous pepsin carboxyl terminus, including a lumenal expansion, a hydrophobic site carrying the transmembrane and cytosolic areas. The lumenal extension spans up to about 35 amino acids and is comprised of secondary structures that directly interact with it by fixing to the pepsin globular catalytic region. Disulfide bonds are attached to both extremes of the lumenal expansion and are directly connected to the catalytic domain. A small sequence of about 11 amino acids secures the catalytic site of BACE1 to the lipid bilayer membrane, C-terminally of the last disul? de bonded cysteine of the luminal expansion. Distant from a hydrophobic region of length of 26 amino

acids including the transmembrane area, another sequence of 21 amino acids expands into the cytoplasm (residues 494–501). This small stretch contains a dileucine chain that interacts with the cytosolic region of APP. BACE1 action can also be controlled by the location of the, a β-sheet hairpin loop that is present over the active site. The active site of ß-secretase is located within the lumen of acidic intracellular compartments. BACE1 is resistant to the inhibitory effect of pepstatin and shows optimal activity at approximately pH 4.5.

In this study, the aim was to carry out drug repurposing by identification of some existing small molecules of unrelated purpose, as potential BACE1 inhibitors using modern in silico tools of drug discovery. Here, we have considered natural compounds imported from ZINC database. Natural products refer to chemical compounds or substances produced by living organisms that is present in the nature. These can be classified into small molecules resulting from metabolic reactions and those obtained as a result of secondary or non-essential metabolism. Natural products are associated with low toxicity. In 2019, nearly 30% of drugs were approved in the US on the basis of drug repurposing.

This practice of drug repurposing has previously been adopted for various disorders such as cardiovascular problems, cancer, obesity, erectile dysfunction, ceasing smoking habits, stress, psychosis, and many other health problems.

Repurposing of drugs decreases the time and cost required for initial screening, toxicity analysis, clinical trials, large-scale manufacturing, and formulation process. In silico-based studies provide much acceptable and results. Although in-silicon drug repurposing methods also have their own advantages, on the other side it has few disadvantages and limitations also. Limitations are related to the data we select for the study. If the volume of data is very less, a proper model cannot be generated, second, it is difficult to understand vague descriptions, third a lack of comprehensive data.

These challenges are associated with drug repurposing methods but can be controlled by software engineering techniques.

2. MATERIALS AND METHODS

2.1. Small Molecules and Protein Structure Preparation

The total numbers of TCM compounds from TCM Database Taiwan were 61,000, and we employed the TCM compounds to search potent ligand as BACE1 inhibitor by docking study. We further used ADMET prediction and Lipinski's rule of five to estimate drug-likeness of the TCM compounds from docking results; these rules make them a likely oral drug in the human body. For ADMET prediction, we based on BBB penetration, CYP2D6 inhibition, and hepatotoxicity to analyze all docked ligands. The crystal structure of BACE1 was taken from PDB database (PDB code: 4JPE); the missing atoms and loops were corrected by Prepare Protein module under Accelrys Discovery Studio 2.5.5.9350 (DS 2.5); residues of BACE1 were protonated in pH 7.4 condition. We also used PONDR-FIT to evaluate unfolded regions on BACE1 sequence for structure validation.

2.2. Docking Study

The volume of BACE1 inhibitor (1M7) in crystal structure of BACE1 was defined as binding site for screening TCM compounds through protein-ligand interaction; different poses of TCM compound were generated by Monte-Carlo techniques; docking study was performed by LigandFit module within DS 2.5. We utilized CHARMm force field to minimize the conformation of each ligand.

$$U(R) = \sum_{\text{bonds}} K_b(b - b_0)^2 + \sum_{\text{angle}} K_\theta(\theta - \theta_0)^2 + \sum_{\text{Urey-Bradley}} K_{\text{UB}}(S - S_0)^2 + \sum_{\text{dihedrals}} K_\varphi(1 + \cos(n\varphi - \delta)) + \sum_{\text{bonds}} K_\omega(\omega - \omega_0)^2 + \sum_{\text{non-bonded pairs}} \{\varepsilon_{ij}^{\min}[(\frac{R_{ij}^{\min}}{r_{ij}})^2 - 2(\frac{R_{ij}^{\min}}{r_{ij}})^6] + \frac{q_i q_j}{4\pi\varepsilon_0 \varepsilon r_{ij}}\} + \sum_{\text{resides}} U_{\text{CMAP}}(\varphi,\psi).$$

Minimization of each docking pose executes 1000 steps of Steepest Descent with an RMS gradient tolerance of 3 and followed by conjugate gradient. The generated conformation of ligands was docked into the defined binding site of BACE1; the ligand poses were calculated by various scoring functions including -PLP1, -PLP2, and -PMF.

2.3. Molecular Dynamics Simulation

The molecular dynamic simulation was carried out by GROMACS 4.5.5 package to simulate the dynamic structure of BACE1 with docked compounds. We utilize charmm27 force field for the simulation system. The distance between the edge of box and protein was set to 1.2 nm. Each protein-ligand system was placed in cubic cell containing water molecular by TIP3P model. Nonbonded interactions include repulsion, dispersion, and Coulomb terms. The repulsion and dispersion terms involve Lennard-Jones interaction and Buckingham potential; the cut-off distance of define van der Waals (VDW) residues was set to 1.4 nm. Long-range electrostatic forces were performed using the PME method.

The equation of Lennard-Jones interaction is as follows:

$$U(r) = 4\varepsilon[(\frac{\delta}{\gamma})^{12} - (\frac{\delta}{\gamma})^6].$$

The Buckingham potential is defined as

$$V_{bh}(r_{ij}) = A_{ij}\exp(-B_{ij}r_{ij}) - \frac{C_{ij}}{R_{ij}^6}.$$

Topology files and parameters of small compounds in protein-ligand complexes were generated for GROMACS simulation by SwissParam web server. Bonds lengths were constrained by the linear constraint solver (LINCS) algorithm. Na^+ and Cl^- ion were randomly replaced with water molecular to neutralize the simulation systems, and the concentration was set as 0.145 M in solvent system. The energy minimization was used to stabilize the solvent system by Steepest Descent algorithm with 5,000 steps, the follow by equilibration performed under position restraints to equilibrated water molecular in the protein for 1 ns under constant temperature dynamics (NVT type) conditions. In final step, production running for 5000 ps under constant pressure and temperature dynamics (NPT type); all of the temperature simulation system was under 310 K condition. MD conformations are sampled every 20 ps and all frames are analyzed under GROMACS 4.5.5.

3. MOLECULAR DYNAMICS

MD is utilized to model ligand-protein complexes when physiologically relevant structures are present. MD stimulation has the advantage of accurately reflecting the real-world conditions of the biological system. Throughout the protein, explicit solvent representation is visible. It forms a highly dynamic protein structure, and the ligand protein complex is solvated with water in the same way that it is in nature. To obtain insight into binding stability and interactions with key amino acids within BACE 1 protein's drug-binding pocket in a dynamic state. MD simulations were performed for three ligand-protein complexes viz., ZINC000150351431-BACE 1 docked complex (complex 1), ZINC000014945921-BACE 1 docked complex (complex 2), ZINC000069488328-BACE 1 docked complex (complex 3) based on molecular docking score, binding energy, IFD score, and oral bioavailability studies. ZINC000049089131, ZINC000261496860, ZINC000069488195, and ZINC000261496858 showed comparatively less binding energy to the target protein.

ZINC000040164523 was found to have poor oral bioavailability. This study was also conducted for the co-crystallized ligand to compare the stability of the ligand-protein complex with the CHEMBL2425609 – protein complex. The frame was captured for 100ps in MD simulation, resulting in 1,000 frames being produced for a 100ns stimulation period and saved in a trajectory. In addition, the stability of the ligand-protein complex was estimated using an RMSD plot (Root mean square deviation) for BACE 1 (4LXM) protein and 'Lig Fit Prot' for the ligands.

For Complex 1 the protein and ligand RMSD values were determined to be within the range of 1.17 Å – 2.00 Å and 1.02 – 4.26, respectively. The complex was stable throughout the study, but a slight drift was observed for a period of 79.6 – 82 ns after which the complex stabilized in the later part of the study (Fig. 2 a). For complex 2, the protein and ligand RMSD values were determined to be within the range of 1.04 Å – 2.07 Å and 1.15 Å – 8.41 Å, respectively, major drifts were observed for 5 – 43 ns and 60 – 100 ns, and during this period the RMSD values were found to be more than the acceptable range of 1–3 Å. For complex 3 the protein and ligand RMSD values were determined to be within the range of 1.02 Å – 1.77 Å and 1.18 Å – 5.81 Å, respectively, initial drift from 0–11 ns was observed due to the initial stabilization of the protein structure with respect to ZINC000069488328 – protein complex and a major drift was observed from 51–53 ns after which the complex stabilized towards the end of the study. For co-crystallised ligand – BACE 1 complex, the protein and ligand RMSD values were determined to be within the range of 1.14 Å – 2.02 Å and 1.14 Å – 2.02 Å, respectively, and slight drift was observed at 93 ns after which the complex stabilized.

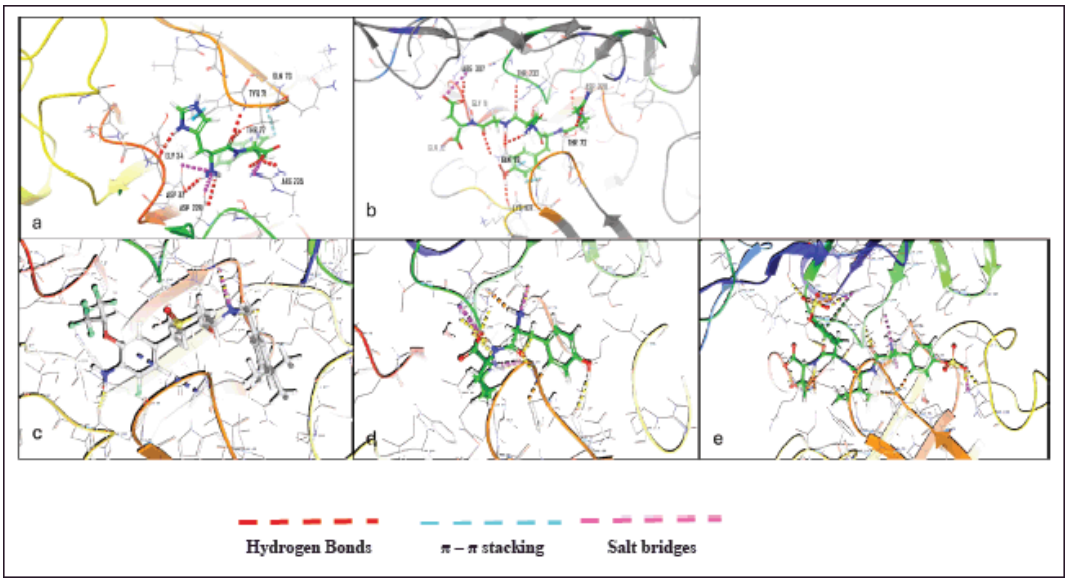

3-D Induced fit docking ligand interactions of a) ZINC000040164523 b) ZINC000014945921 c) CHEMBL2425609 d) ZINC000069488328 e) ZINC000150351431 BACE 1 (4LXM) protein and 'Lig Fit Prot' for the ligands.

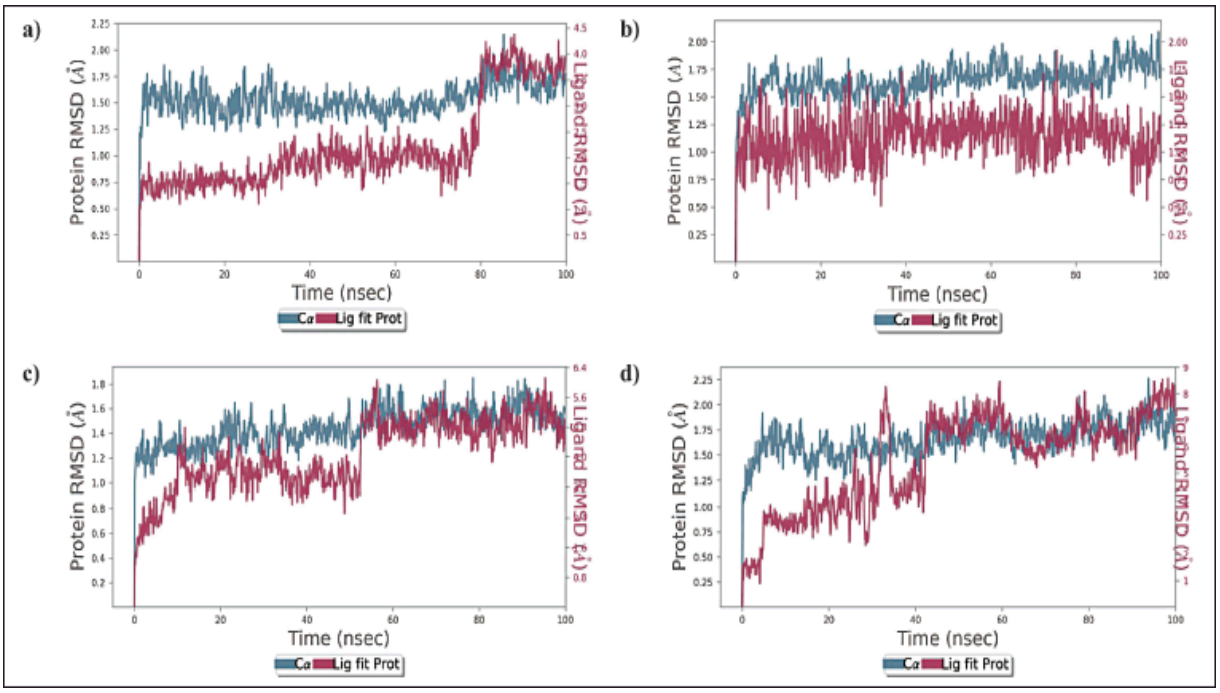

RMSD plot of ZINC000150351431 and BACE 1 protein complex b) RMSD plot of ZINC000014945921 and BACE 1 protein complex c) RMSD plot of ZINC000069488328 and BACE 1 protein complex d) RMSD plot of CHEMBL2425609 (co-crystallised ligand) and BACE 1 protein complex.

Throughout the simulation study, the protein-ligand interactions were also monitored, and an analysis report was generated for the potential protein-ligand interactions. In the chosen trajectory, interactions that occur more than 30.0% of the simulation time were noted. Complex 1 made hydrogen bond interactions with ARG128, SER325, ARG235, GLN73, THR232, GLY230, THR231, ASP228, ASP32, and THR72. The π-cation interaction was made with ARG235.

Hydrophobic interactions were also present but with weaker occupancy with LEU30, TYR71, and ARG235. Complex 2 made hydrogen bond interactions with Thr232 and Asp32. Water bridged interactions were seen with LYS107 and THR72, also hydrophobic interactions with weaker occupancy were seen with LEU30, TYR71, PHE108, ILE110, and TRP115. Complex 3 made hydrogen bond interactions with Thr72, Asp32, ASP228, and PRO70. It made water bridges interaction with ASP228 and π-π stacking interactions with TYR71. Hydrophobic interactions were observed with TYR71 and PRO70. Co-crystallised ligand–BACE 1 complex made hydrogen-bonding interactions with ASP228, ASP32, GLY34, and PHE108. π-π stacking was observed with TYR71 and hydrophobic interactions were seen with PHR108 and TYR71.

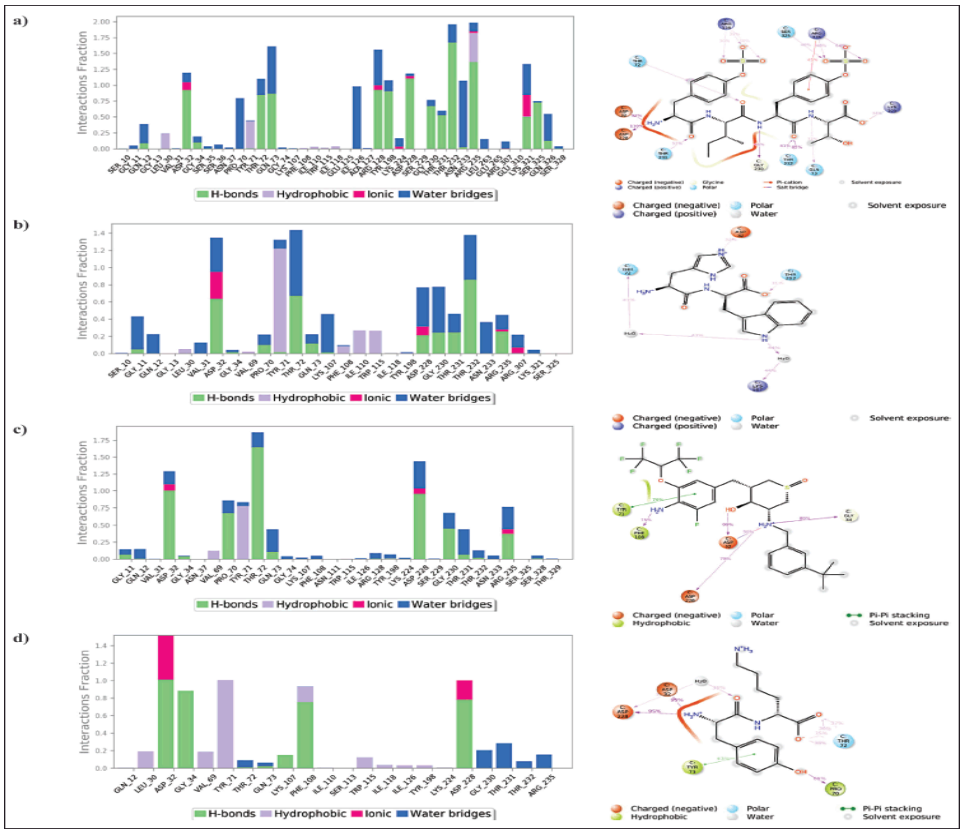

Histogram of protein-ligand interactions. (a) Interaction of ZINC000150351431 with various BACE 1 protein residues (b) Interaction of ZINC000014945921 with various BACE 1 protein residues(c) Interaction of ZINC000069488328 with various BACE 1 protein residues (d) Interaction of CHEMBL2425609 (co-crystallized ligand) with various BACE 1 protein residues. The percentage of simulation time that a specific contact is maintained is represented by the value less than 1 in the stacked bar chart. A value greater than 1.0 implies that the same protein residue interacts with the ligand many times.

S.No	Compounds	H-bond interactions		Hydrophobic interactions		π-π stacking		IFD Score(kcal/mol)
		New	Missing	New	Missing	New	Missing	
1	CHEMBL2425609	ARG235	ASP32	-	-	TYR198	-	−794.42
2	ZINC000150351431	SER325 GLY11 GLN73	ASP228	—	—	—	TYR71	−803.50
3	ZINC000040164523	GLN12 GLN73 THR72 LYS107	PHE108 GLY34 TYR19	—	PHE109 PRO70	TRP115	—	−807.13
4	ZINC000069488328	THR72 ARG235 PRO70	GLN73 LYS107	PRO70 VAL69 TYR198 ILE226 VAL332	—	—	PHE108	−794.29
5	ZINC000014945921	ARG235 PHE108	-	PHE108 ILE110 TRP115 LEU30	VAL332 ALA127	TYR71	-	−795.24
6	ZINC000049089131	LYS107	ASP228	-	-	TYR71	-	−793.26
7	ZINC000261496860	LYS321 ARG235 THR72 GLY264	LYS224 ASP228	PRO70 PHE322 ILE110	VAL332 ILE226	-	-	−803.30
8	ZINC000069488195	GLN73	-		ILE126	TYR71	-	−794.92
9	ZINC000261496858	ARG235 THR72 ILE126	GLN73 TYR198 ASP228 ARG307	VAL332 ILE110 ALA127 VAL69 TYR71	LEU30 ALA323	—	—	−804.80

P-RMSF (Protein root mean square fluctuations) was utilized to visualize the fluctuations of each protein residue across the simulated time period. The protein amino acid residue that fluctuates more is represented by higher peaks. For complex 1, the most fluctuating residues were observed to be ALA313 with an RMSF value of 2.58 Å, GLN73 with RMSF value of 2.55 Å and GLY273 with RMSF value of 2.56 Å. RMSF of the remaining protein was found within the range of 1.02 Å to 2.58Å. For complex 2, the most fluctuating residues were observed to be VAL312 with RMSF value of 3.42 Å, SER46 with RMSF value of 3.00 Å and ALA157 with RMSF value of 3.00 Å. RMSF values of remaining protein was found within the range of 0.67 Å–3.42 Å. For complex 3, the most volatile residues were observed to be SER46 with RMSF value of 2.32 Å and ALA313 with RMSF value of 2.40 Å. RMSF volatility for remaining protein was found within the range of 0.56 Å–3.32 Å. For complex 4, the most volatile residues were observed to be THR314 with RMSF value of 4.06 Å, ASP311 with RMSF value of 2.89 Å and LEU167. RMSF volatility for remaining protein was found within the range of 0.60 Å–4.06 Å.

Ligand root mean square fluctuation (L-RMSF) could reveal how ligand fragments interact with proteins and have an entropic function in the binding process. For complex 1, O groups at position 34 and position 35 of the ring B of the structure were found to be the most volatile with an RMSF value of 4.43 Å and 4.37 Å, respectively. Other major fluctuations were seen with O atom at position 36 of ring B with an RMSF value of 4.01 Å. Overall the RMSF value of complex 1 with respect to protein ligand complex was observed within the range of 0.94 Å–4.43 Å. For complex 2, major volatility was seen with C alkene (position 7) of the imidazolinium ring with an RMSF value of 3.64 Å and with NH ion (position 6) of the imidazolinium ring with an RMSF value of 3.59 Å. Overall the RMSF value of complex 2 with respect to protein ligand complex was observed within the range of 2.14 Å–3.64 Å. For complex 3 major volatility was seen with NH group at position 1 with an RMSF value of 6.73 Å and with C atoms at positions 2, 3 and 4 with RMSF values of 5.78 Å, 4.88 Å and 3.80 Å, respectively. Overall, the RMSF value of complex 2 with respect to protein ligand complex was observed within the range of 0.67 Å–6.73 Å. For co-crystallized ligand—BACE 1, complex major volatility was seen with F (fluorine) atoms at position 1, 3, 4 with RMSF values of 2.29 Å, 2.34 Å, 2.15 Å, respectively.

Overall, the RMSF value of co-crystallized ligand—BACE 1 complex with respect to protein ligand complex was observed within the range of 0.53 Å–2.36 Å. After a thorough analysis it was found out that aromatic ring, amine, and ketone groups were important structural features required for good interactions with the protein complex.

4. RESULTS AND DISCUSSION

4.1. Docking Results

We utilize PONDR-FIT to understand the amino acids on binding region (GLN60, GLY61, ASP80, ILE158, ILE166, ASP276, GLY278, and THR279) of BACE1 are not disorder structure, and the values of disorder disposition are below 0.5, which indicate that the binding site of BACE1 is order structure, and the ligands binding may not affected by protein structure. For docking analysis, we based on -PLP1, -PLP2, and -PMF to evaluate the docking pose of traditional Chinese medicine (TCM) compounds. From scoring analysis, pyrimidine analogue R-50 (1M7) was regarded as control for comparison, which is synthesis BACE1 inhibitor from Hunt's study. Top candidates with higher values of scores than 1M7. For ADMET evaluation, all TCM candidates have no CYP2D6 inhibited and hepatotoxicity, suggesting that CYP2D6 may not be affected by these ligands in liver. The 1M7 has hepatotoxicity in ADMET analysis, indicating that our TCM candidates are safer than control. All docked ligands are ranked by -PMF score, due to the prediction of blood-brain barrier (BBB) penetration showing Diterpenoid EF-D with no penetration ability (BBB

level = 4); the Triptofordin B1 has -PMF score (194.61) and medium penetration (BBB level = 2), which is better than 1M7 because of the low penetration (BBB level = 3) and low binding score (-PMF = 119.39). Triptofordin B1 is available in Tripterygium wilfordii; the herb extraction has therapeutic effect for SAMP8 mice with AD disease. So we selected Triptofordin B1 for further studies; the chemical scaffolds of TCM candidates and 1M7 . Docking pose of Triptofordin B1 displayed pi-pi interaction with TYR119; close residues include ASP80 and ASP276. 1M7 binding pose has H-bond with ASP80 and ASP276, but there is no pi interaction presented between residue and ligand. The data reveal that Triptofordin B1 has similar binding position with 1M7 and displayed stronger chemical interaction in BACE1 binding site. In further study, we utilized MD simulation to perform dynamic protein-ligand complexes for variation analysis.

Name	-PLP1	-PLP2	-PMF	BBB Level	CYP2D6	Hepatotoxicity
Diterpenoid EF-D	79.04	75.67	195.32	4	0	0
Triptofordin B1	*68.44*	*62.28*	*194.61*	*2*	*0*	*0*
Shionoside C	71.67	69.36	193.84	4	0	0
Jangomolide	72.27	67.01	187.36	3	0	0
Vibsanin W	77.98	76.62	184.31	4	0	0
2α,6α-Dihydroxybetulinic acid	59.52	57.72	183.93	2	0	0
Benzoylramanone	63.59	61.05	183.67	2	0	0
Pseurata D	63.28	62.87	180.42	4	0	0
Vibsanin I	78.18	72.43	179.15	4	0	0
1M7*	**70.70**	**52.10**	**119.39**	**3**	**0**	**1**

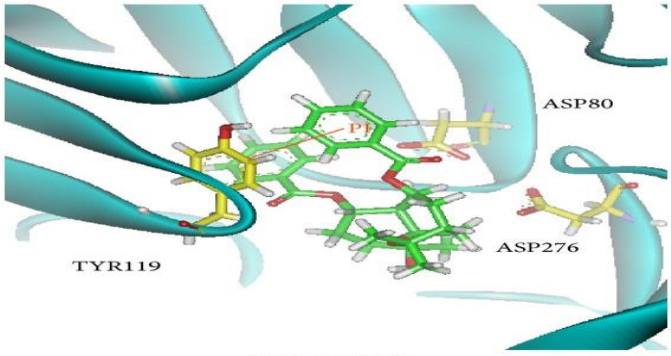

Triptofordin B1

(a)

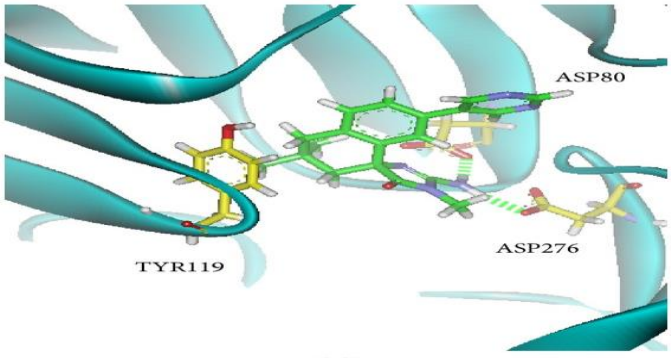

1M7

(b)

The docking poses of small compounds: (a) Triptofordin B1; (b) 1M7. Small compound and amino acids are colored in green and yellow, respectively.

4.2. Stability Analysis

Structure of BACE1 with docked ligands includes Triptofordin B1 and 1M7 that were carried out by MD simulation, and we use protein structure of BACE1 with no ligand (Apoprotein) for comparison. The analysis result of protein root mean square deviation (RMSD) and radius of gyration (Rg). 1M7 displayed fluctuation from 500 to 4500 ps and was stable at 0.3 nm of protein RMSD. Triptofordin B1 and Apoprotein show similar trends; the protein RMSD remained stable in the region of 0.3 nm. The radius of gyration (Rg) analysis shows that the compactness of BACE1 with each ligand is less than the Apoprotein structure, because of the docked ligand combined with BACE1. From 3000 to 5000 ps of Rg analysis, the structure tends to be stable around 0.4 nm.

We further analyzed RMSD of each small molecular during MD simulation; ligand RMSD of Triptofordin B1 and 1M7 increases large fluctuation at 2000 ps; the value of ligand RMSD increased from 0.04 to 0.10 nm. Interestingly, 1M7 is decreased from 0.10 nm 0.04 nm after 4500 ps; this finding suggests that the region of 2000 to 4000 ps should be used to analyze the conformation of ligand binding. For total energy analysis, there significant increased values were observed at initial simulation time; the total energy is remained around -8.74×106 kJ/mol for 1M7 and Apoprotein; the Triptofordin B1 was stable at -8.72×105 kJ/mol. These results suggest that all structures of the complexes remained constant after initial simulation time; there is no significant fluctuation among all BACE1 structures.

4.3. Residues Fluctuation Analysis on the Binding Region

We using root mean squared fluctuation (RMSF) to analyze the fluctuation of residues on protein binding site; the binding region (GLN60, GLY61, ASP80, ILE158, ILE166, ASP276, GLY278, and THR279) shows small flexibility. The largest fluctuation is observed from 425 to 450 residues, because these regions are far away from the binding site, indicating that the flexible amino acids do not affect protein-ligand interaction during MD simulation.

According to DSSP analysis, the number of helix and beta-sheet remained 150 and 100, respectively; the other secondary type also revealed no distinct changes. Besides, the distance for pair of each residue has no missing plot among all BACE1 structures during 5000 ps,. The results show that structure of BACE1 remained constant during all MD simulations.

4.4. Movement of Each Ligand Analysis

The mobility of each ligand was analyzed by mean square displacement (MSD); Triptofordin B1 increased MSD values to 0.3 nm at 2500 ps, and stabilizes until 4000 ps. 1M7 was stable below 0.1 nm and decreased MSD value at 4500 ps. In final simulation after 4500 ps, Triptofordin B1 further increased MSD values to 0.45 nm and tends to be stable to the end time. Here, we further analyze the distance between BACE1 and each ligand among 5000 ps. The distance between 1M7 and BACE1 displayed 1.00 nm before 2000 ps, but Triptofordin B1 increased to 1.50 nm from 2000 to 3500 ps, and the other wild increased distance occur from 4000 to 5000 ps. These results comparing with MSD analysis;the region of 200 to 3500 ps has significant change during dynamics simulation; in the next analysis, we focus on these regions of simulation time for further studies.

4.5. Clustering Analysis for Snapshot Observing

In order to understand the most stable structure during the entire MD simulation for understanding the movement of BACE1, all frames of MD simulation were clustered into different subgroups; the similar MD conformations were grouped into the same cluster. For clustering results, each last group includes last 1000 ps (from 4000 to 5000 ps); hence, we selected the middle flams from each last group for further analysis from all MD complexes. Before observing all snapshots from middle frames of last clustering group, we also calculate the distance of H-bonds for each ligand among all simulation times; GLN121 showed decreased distance after 4000 ps for Triptofordin B1. ASP80 and ASP276 remain revealed low distance with 1M7, suggesting that GLN121, ASP80, and ASP276 are essential amino acid for ligand binding. In snapshot analysis, we found that Triptofordin B1 could reduce the binding site, because the GLN121 has significant change, and presenting pi interaction with TRP163, and in ligand channel analysis, we can see that the predicted channel of Triptofordin B1 is shorter than 1M7 and Apoprotein, suggesting that Triptofordin B1 could bind to BACE1 better than 1M7.

5. CONCLUSION

For ADMET analysis, Triptofordin B1 has more penetration than 1M7 and less toxicity, because 1M7 has hepatotoxicity in ADMET prediction. Three scoring functions, -PLP1, -PLP2, and –PMF, are higher than control. The structure of BACE1 analysis shows that the binding residues have less fluctuation after MD simulations, indicating the each ligand is not affected by protein residues. In migration analysis for Triptofordin B1 and 1M7, the stable region displayed from 3000 to 4000 ps; we utilize clustering analysis to observe this period simulation time. Triptofordin B1 could reduce the binding cavity of BACE1; the results reveal that Triptofordin B1 could bind to BACE1 and better than 1M7, which could be used as potential lead drug to design novel BACE1 inhibitor for AD therapy

ACKNOWLEDGMENTS

The research was supported by grants from the National Science Council of Taiwan (NSC102-2325-B039-001, NSC102-2221-E-468-027-), Asia University (ASIA100-CMU-2, ASIA101-CMU-2, 102-ASIA-07), and China Medical University Hospital (DMR-103-058, DMR-103-001, DMR-103-096). This study is also supported in part by Taiwan Department of Health Clinical Trial and Research Center of Excellence (DOH102-TD-B-111-004) and Taiwan Department of Health Cancer Research Center of Excellence (MOHW103-TD-B-111-03).

REFERENCES

1. Mokhtar SH, Bakhuraysah MM, Cram DS, Petratos S. The beta-amyloid protein of alzheimer's disease: communication breakdown by modifying the neuronal cytoskeleton. International Journal of Alzheimer’s Disease, 2013; 2013: 15 pages. doi: 10.1155/2013/910502.9105
2. Grimm MO, Mett J, Stahlmann CP, et al. Neprilysin and abeta clearance: impact of the APP intracellular domain in NEP regulation and implications in Alzheimer's disease. Frontiers in Aging Neuroscience, 2013; 5, article 98 doi: 10.3389/fnagi.2013.00098.
3. Petrella JR. Neuroimaging and the search for a cure for Alzheimer disease. Radiology, 2013; 269(3): 671–691. doi: 10.1148/radiol.13122503.
4. Weinstein JD, Gonzalez ER, Egleton RD, Hunt DA. A paradigm shift for evaluating pharmacotherapy for Alzheimer's disease: the 10-patient screening protocol. The Consultant Pharmacist, 2013; 28(7): 443–454. doi: 10.4140/TCP.n.2013.443.

5. Ghezzi L, Scarpini E, Galimberti D. Disease-modifying drugs in Alzheimer's disease. Drug Design, Development and Therapy, 2013; 7: 1471–1479. doi: 10.2147/DDDT.S41431.
6. Duyckaerts C, Delatour B, Potier M-C. Classification and basic pathology of Alzheimer disease. Acta Neuropathologica, 2009; 118(1): 5–36. doi: 10.1007/s00401-009-0532-1.
7. Querfurth HW. Calcium ionophore increases amyloid β peptide production by cultured cells. Biochemistry, 1994; 33(15): 4550–4561. doi: 10.1021/bi00181a016.
8. Morgan D, Diamond DM, Gottschall PE, et al. A β peptide vaccination prevents memory loss in an animal model of Alzheimer's disease. Nature, 2000; 408(6815): 982–985. doi: 10.1038/35050116.
9. McLaurin J, Cecal R, Kierstead ME, et al. Therapeutically effective antibodies against amyloid-β peptide target amyloid-β residues 4-10 and inhibit cytotoxicity and fibrillogenesis. Nature Medicine, 2002; 8(11): 1263–1269.
10. Philippe B, Brion J-P, Macq A-F, Octave J-N. A new monoclonal antibody against the anionic domain of the amyloid precursor protein of Alzheimer's disease. NeuroReport, 1993; 5(3): 289–292. doi: 10.1097/00001756-199312000-00027.
11. Wilcock DM, Rojiani A, Rosenthal A, et al. Passive immunotherapy against Aβ in aged APP-transgenic mice reverses cognitive deficits and depletes parenchymal amyloid deposits in spite of increased vascular amyloid and microhemorrhage. Journal of Neuroinflammation, 2004;1(1, article 24) doi: 10.1186/1742-2094-1-24.
12. Wisniewski T, Konietzko U. Amyloid-β immunisation for Alzheimer's disease. The Lancet Neurology, 2008; 7(9): 805–811. doi: 10.1016/S1474-4422(08)70170-4.
13. Rasool S, Albay R, Martinez-Coria H, et al. Vaccination with a non-human random sequence amyloid oligomer mimic results in improved cognitive function and reduced plaque deposition and micro hemorrhage in Tg2576 mice. Molecular Neurodegeneration, 2012; 7, article 37 doi: 10.1186/1750-1326-7-37.
14. Selkoe DJ, Wolfe MS. Presenilin: running with Scissors in the membrane. Cell, 2007; 131(2): 215–221. doi: 10.1016/j.cell.2007.10.012.
15. Yin M-C. Anti-glycative potential of triterpenes: a mini-review. BioMedicine, 2012; 2(1): 2–9.
16. Butini S, Gabellieri E, Brindisi M, et al. A stereoselective approach to peptidomimetic BACE1 inhibitors. European Journal of Medicinal Chemistry, 2013; 70: 233–247. doi: 10.1016/j.ejmech.2013.09.056.
17. Zou Y, Xu L, Chen W, et al. Discovery of pyrazole as C-terminus of selective BACE1 inhibitors. European Journal of Medicinal Chemistry, 2013; 68: 270–283. doi: 10.1016/j.ejmech.2013.06.027.
18. Eketjall S, Janson J, Jeppsson F, et al. AZ-4217: a high potency BACE inhibitor displaying acute central efficacy in different in vivo models and reduced amyloid deposition in Tg2576 mice. The Journal of Neuroscience, 2013; 33(24): 10075–10084. doi: 10.1523/JNEUROSCI.1165-13.2013.
19. Huang H-J, Yu HW, Chen C-Y, et al. Current developments of computer-aided drug design. Journal of the Taiwan Institute of Chemical Engineers, 2010; 41(6): 623–635.
20. Chen CY. A novel integrated framework and improved methodology of computer-aided drug design. Current Topics in Medicinal Chemistry, 2013; 13(9): 965–988. doi: 10.2174/1568026611313090002.
21. Tsai T-Y, Chang K-W, Chen CY-C. IScreen: world's first cloud-computing web server for virtual screening and de novo drug design based on TCM database@Taiwan. Journal of Computer-Aided Molecular Design, 2011; 25(6): 525–531. doi: 10.1007/s10822-011-9438-9.

22. Chang K-W, Tsai T-Y, Chen K-C, et al. iSMART: an integrated cloud computing web server for traditional Chinese medicine for online virtual screening, de novo evolution and drug design. Journal of Biomolecular Structure and Dynamics, 2011; 29(1): 243–250. doi: 10.1080/073911011010524988.
23. Chen CY-C. TCM Database@Taiwan: the world's largest traditional Chinese medicine database for drug screening In Silico. PLoS ONE, 2011; 6(1) doi: 10.1371/journal.pone.0015939.e15939
24. Lin P-C, Liu P-Y, Lin S-Z, Harn H-J. Angelica sinensis: a Chinese herb for brain cancer therapy. BioMedicine, 2012; 2(1): 30–35.
25. Hsu SC, Lin JH, Weng SW, et al. Crude extract of Rheum palmatum inhibits migration and invasion of U-2 OS human osteosarcoma cells by suppression of matrix metalloproteinase-2 and -9. BioMedicine, 2013; 3(3): 120–129.
26. Hsu SC, Chung JG. Anticancer potential of emodin. BioMedicine, 2012; 2(3): 108–116. doi: 10.1016/j.biomed.2012.03.003.
27. Chen KC, Chang SS, Tsai FJ, Chen CY. Han ethnicity-specific type 2 diabetic treatment from traditional Chinese medicine? Journal of Biomolecular Structure and Dynamics, 2013; 31(11): 1219–1235. doi: 10.1080/07391102.2012.732340.
28. Tou WI, Chang SS, Lee CC, Chen CY. Drug design for neuropathic pain regulation from traditional Chinese medicine. Scientific Reports, 2013; 3, article 844 doi: 10.1038/srep00844.